

2013

Trex1 regulates lysosomal biogenesis and interferon-independent activation of antiviral genes

Maroof Hasan

University of Texas Southwestern Medical Center

James Koch

University of Texas Southwestern Medical Center

Dinesh Rakheja

University of Texas Southwestern Medical Center

Asit K. Pattnaik


University of Nebraska-Lincoln, apattnaik2@unl.edu

James Brugarolas

University of Texas Southwestern Medical Center

See next page for additional authors

Follow this and additional works at: <http://digitalcommons.unl.edu/vetscipapers>

 Part of the [Biochemistry, Biophysics, and Structural Biology Commons](#), [Cell and Developmental Biology Commons](#), [Immunology and Infectious Disease Commons](#), [Medical Sciences Commons](#), [Veterinary Microbiology and Immunobiology Commons](#), and the [Veterinary Pathology and Pathobiology Commons](#)

Hasan, Maroof; Koch, James; Rakheja, Dinesh; Pattnaik, Asit K.; Brugarolas, James; Dozmorov, Igor; Levine, Beth; Wakeland, Edward K.; Lee-kirsch, Min Ae; and Yan, Nan, "Trex1 regulates lysosomal biogenesis and interferon-independent activation of antiviral genes" (2013). *Papers in Veterinary and Biomedical Science*. 220.

<http://digitalcommons.unl.edu/vetscipapers/220>

This Article is brought to you for free and open access by the Veterinary and Biomedical Sciences, Department of at DigitalCommons@University of Nebraska - Lincoln. It has been accepted for inclusion in Papers in Veterinary and Biomedical Science by an authorized administrator of DigitalCommons@University of Nebraska - Lincoln.

Authors

Maroof Hasan, James Koch, Dinesh Rakheja, Asit K. Pattnaik, James Brugarolas, Igor Dozmorov, Beth Levine, Edward K. Wakeland, Min Ae Lee-kirsch, and Nan Yan



HHS Public Access

Author manuscript

Nat Immunol. Author manuscript; available in PMC 2013 July 01.

Published in final edited form as:

Nat Immunol. 2013 January ; 14(1): 61–71. doi:10.1038/ni.2475.

Trex1 regulates lysosomal biogenesis and interferon-independent activation of antiviral genes

Maroof Hasan^{1,2}, James Koch^{1,2}, Dinesh Rakheja³, Asit K. Pattnaik^{4,5}, James Brugarolas^{1,6,7}, Igor Dozmorov⁸, Beth Levine^{1,2,9,10}, Edward K. Wakeland⁸, Min Ae Lee-kirsch¹¹, and Nan Yan^{1,2}

¹Department of Internal Medicine, University of Texas Southwestern Medical Center, Dallas, Texas, USA

²Department of Microbiology, University of Texas Southwestern Medical Center, Dallas, Texas, USA

³Department of Pathology, Children's Medical Center, University of Texas Southwestern Medical Center, Dallas, Texas, USA

⁴School of Veterinary Medicine and Biomedical Sciences, University of Nebraska, Lincoln, Nebraska, USA

⁵Nebraska Center for Virology, University of Nebraska, Lincoln, Nebraska, USA

⁶Department of Developmental Biology, University of Texas Southwestern Medical center, Dallas, Texas, USA

⁷Simmons Cancer Center, University of Texas Southwestern Medical Center, Dallas, Texas, USA

⁸Department of Immunology University of Texas Southwestern Medical center, Dallas, Texas, USA

⁹Center for Autophagy Research, University of Texas Southwestern Medical Center, Dallas, Texas USA

¹⁰Howard Hughes Medical Institute, University of Texas Southwestern Medical Center, Dallas, Texas, USA

¹¹Children's Hospital, Technical University Dresden, Dresden, Germany

Abstract

Innate immune sensing of viral nucleic acids triggers type I interferon (IFN) production, which activates interferon-stimulated genes (ISGs) and directs a multifaceted antiviral response. ISGs can also be activated through IFN-independent pathways, although the precise mechanisms remain

Users may view, print, copy, download and text and data- mine the content in such documents, for the purposes of academic research, subject always to the full Conditions of use: http://www.nature.com/authors/editorial_policies/license.html#terms

Correspondence should be addressed to N.Y., nan.yan@utsouthwestern.edu.

AUTHOR CONTRIBUTIONS

M.H. and N.Y. designed and performed most experiments; J.K. helped do the experiments; M.L.-K. provided human cells and scientific advice; D.R. performed EM analysis. A.K.P. and B.L. contributed reagents and scientific advice; E.K.W. and I.D. helped analyze the data; M.H. and N.Y. wrote the paper.

elusive. Here we found that the cytosolic exonuclease Trex1 regulates the activation of a subset of ISGs independently of IFN. Both *Trex1*^{-/-} mouse and *TREX1*-mutant human cells express high levels of antiviral genes and are refractory to viral infections. The IFN-independent activation of antiviral genes in *Trex1*^{-/-} cells requires STING, TBK1 and IRF3 and IRF7. We also found that Trex1-deficient cells display expanded lysosomal compartment, altered subcellular localization of the transcription factor EB (TFEB), and reduced mTORC1 activity. Together, our data identify Trex1 as a regulator of lysosomal biogenesis and IFN-independent activation of antiviral genes, and shows dysregulation of lysosomes can elicit innate immune responses.

Vertebrates are constantly facing challenges from pathogenic microbes that introduce a variety of microbial proteins and nucleic acids into the host cell. To counter this, eukaryotic cells express many different pattern-recognition receptors (PRRs) that detect microbial pathogen-associated molecular patterns (PAMP), which then activate antiviral interferon (IFN) and proinflammatory responses¹. Mammalian PRRs include Toll-like receptors (TLRs), RIG-I-like receptors (RLRs), NOD-like receptors (NLRs), C-type lectin receptors (CLRs), and an emerging category of cytosolic DNA receptors². In the case of viral infection, viral nucleic acids are the major PAMP detected by the host innate immune receptors, which include RLRs and DNA receptors in the cytosol and a subfamily of TLRs that localize to the endosomal membrane³. The central hub for cytosolic DNA sensing is the endoplasmic reticulum (ER) membrane protein STING (also known as MITA, MPYS or ERIS)². A number of proteins have been proposed to detect double-stranded DNA in the cytosol and signal through STING, such as DAI, IFI16 and DDX41⁴⁻⁶. STING can also directly recognize c-di-GMP, which is usually associated with bacterial infection and activates IFN expression⁷. Although IFN plays a major role in controlling viral infections, IFN-independent pathways also exist and are vital for antiviral defense. For example, STING can activate STAT6 independently of the IFN pathway; and activated STAT6 induces chemokine expression that primes adaptive immune responses⁸. Infection with enveloped viruses also triggers an IFN-independent pathway that involves the direct activation of a subset of IFN stimulatory genes (ISG) by IRF3⁹. A recent study of MAVS-mediated innate immune responses to RNA viruses demonstrated that IFN-independent induction of antiviral genes occurs rapidly after infection and is functionally important for controlling viral replication before the onset of more robust and sustained IFN activation¹⁰.

Innate immune sensing pathways are carefully designed to distinguish self- versus non-self ligands, either by spatial separation (e.g. TLR7 and TLR9 reside in endosomes which are devoid of host nucleic acids), or by stringent ligand specificity (e.g. TLR9 recognizes CpG-containing DNA in bacteria; RIG-I recognizes 5'-ppp-containing RNA in viruses). However, how cytosolic DNA sensing pathways distinguish host and viral DNA remains unclear. We have previously identified Trex1, an exonuclease that resides on the ER, as a negative regulator of innate immune sensing of cytosolic HIV DNA. In *Trex1*^{-/-} mouse embryonic fibroblasts or human CD4⁺ T cells and macrophages in which Trex1 was depleted by RNAi, cytosolic HIV DNA accumulated and triggers IFN through the STING-TBK1-IRF3 pathway¹¹. These findings and other studies¹² suggest that cells rely on negative regulatory mechanisms such as Trex1 to keep cytosolic DNA sensing pathways in check.

Trex1 deficiency has been implicated in the pathogenesis of autoimmunity. *TREX1* mutations in humans are associated with a spectrum of autoimmune and inflammatory phenotypes including Aicardi-Goutières syndrome (AGS, an inflammatory brain disease that mimics the symptoms of congenital viral infection^{13,14}), systemic lupus erythematosus (SLE), familial chilblain lupus (FCL) and retinal vasculopathy with cerebral leukodystrophy (RVCL)^{15–17}. *TREX1* mutations were found in up to 2% of SLE patients with an extremely high odds ratio (OR=25)¹⁸, representing one of the highest disease risk recorded for a single susceptibility gene in complex polygenic SLE¹⁴. Studies using *Trex1*^{-/-} mice revealed that *Trex1*^{-/-} cells accumulate cytosolic ssDNA that might be derived from DNA repair in the nucleus or from endogenous retroelements^{19,20}. Recent genetic evidence demonstrated that the STING-mediated DNA sensing pathway is essential for the pathogenesis of autoimmune disease in *Trex1*^{-/-} mice¹². Initiation of IFN expression is only detected in a subset of non-hematopoietic cells in *Trex1*^{-/-} mice, raising the question of what happens to the majority of other cells that also lack Trex1 function. We also wondered whether Trex1 inhibits IFN responses to other viruses besides HIV, and/or if the mere loss of Trex1 function in a cell would elicit innate immune responses and establish an antiviral state?

In this study, we found that Trex1-deficient or mutant cells display broad antiviral activity against many RNA viruses. The antiviral activity comes from elevated expression of ISGs in cells that lack Trex1 function, and is mediated through an IFN-independent signaling pathway that involves STING-TBK1-IRF3-IRF7. We also found that Trex1 regulates lysosomal biogenesis through TFEB and mTORC1 pathway, and provided evidence that dysregulation of lysosomes elicits innate immune response.

RESULTS

Impaired VSV replication in Trex1 deficient cells

To investigate whether Trex1 is involved in the IFN response to RNA viruses, we infected wild-type (WT) and *Trex1*^{-/-} MEFs with vesicular stomatitis virus (VSV, Indiana strain), a negative stranded RNA virus, with VSV-G pseudotyped HIV¹¹, or with a mock infection, and measured levels of IFN- β mRNA 24 h post infection (hpi). As previously reported¹¹, mock-infected WT and *Trex1*^{-/-} cells did not express detectable levels of IFN- β mRNA, and HIV infection only stimulated IFN- β mRNA expression in *Trex1*^{-/-} cells, but not in WT cells. In contrast, VSV infection stimulated strong IFN- β mRNA expression in both WT and *Trex1*^{-/-} cells at similar levels (Fig. 1a), suggesting that Trex1 does not regulate the Type I IFN response to VSV. However, VSV replication was severely impaired in *Trex1*^{-/-} cells compared to WT, even though IFN- β induction was indistinguishable between the two cell types (Fig. 1b–d). Specifically, mRNA levels of two major forms of VSV RNA, G and M, were reduced to 12% and 7% (of WT), respectively, in *Trex1*^{-/-} as compared to in WT cells (Fig. 1b). We also detected markedly reduced amounts of VSV proteins in *Trex1*^{-/-} as compared to in WT cells, using two different multiplicities of infection (MOI, 2 and 10) (Fig. 1c). VSV titers from infected *Trex1*^{-/-} cells were also reduced compared to WT (Fig. 1d). To better quantify and visualize VSV replication, we infected WT and *Trex1*^{-/-} cells with VSV-PeGFP, in which eGFP was fused in-frame to the VSV P protein that is usually associated with viral RNA replication foci in the cell²¹. We observed reduced VSV-PeGFP

replication (14% of WT) in *Trex1*^{-/-} cells compared to WT cells by fluorescence-activated cell sorting (FACS) analysis (Fig. 1e).

Consistent with our FACS data, fluorescent microscopy analysis of infected WT cells revealed bright replication foci marked by PeGFP, whereas very little green fluorescent signal was detected in VSV-PeGFP infected *Trex1*^{-/-} cells (Fig. 1f). We also infected bone marrow-derived macrophages (BMDMs) generated from WT, *Trex1*^{+/-} and *Trex1*^{-/-} mice and found that only *Trex1*^{-/-} cells were resistant to VSV infection (Fig. 1g, h).

We next examined whether VSV entry is inhibited in *Trex1*^{-/-} cells. This seemed unlikely as *Trex1*^{-/-} cells did not inhibit entry of VSV-G pseudotyped HIV¹¹, and VSV infection stimulated indistinguishable levels of IFN mRNA expression in WT and *Trex1*^{-/-} cells (Fig. 1a). Nonetheless, to rule out the possibility of an entry defect, we labeled wild type VSV virions with a fluorescent dye DiL and followed the infection of VSV-DiL in WT and *Trex1*^{-/-} cells by live cell fluorescence microscopy (Supplementary Fig. 1a). We observed no differences in intracellular VSV-DiL comparing WT and *Trex1*^{-/-} cells at 1 hpi. We also observed similar levels of VSV G and M RNA at 1 hpi in both cell types (Supplementary Fig. 1b). These data suggest that VSV replication was blocked at an early stage post entry, such as uncoating or RNA replication, in *Trex1*^{-/-} cells. We also found that in contrast to infected WT cells, VSV infected *Trex1*^{-/-} cells did not show detectable cytopathic effects (Supplementary Fig. 2), consistent with the notion that *Trex1*^{-/-} cells were protected against viral infection.

To investigate whether Trex1 is also required for VSV replication in human cells, we infected WT and *TREX1*^{R114H/R114H} (*TREX1*-mutant) skin fibroblasts from an AGS patient with VSV or VSV-PeGFP and measured levels of viral RNA. Arginine 114 is a critical residue at the interface of the Trex1 dimer, and the R114H mutation severely disrupts Trex1 function *in vitro*²². R114H represents the most common Trex1 mutation in patients with AGS, and has also been associated with SLE¹⁴. Both VSV and VSV-PeGFP infection was decreased in *TREX1*^{R114H/R114H} cells compared to WT cells, as reflected by reduced levels of viral RNA, reduced amounts of viral proteins, and reduced numbers of viral replication foci (Fig. 1i-k). Taken together, we conclude that VSV replication is impaired at an early post entry step in both mouse and human cells lacking Trex1 function.

Trex1 deficient cells display broad antiviral resistance

To determine whether the replication block in *Trex1*^{-/-} and *TREX1*^{R114H/R114H} cells was unique for VSV, we infected WT and *Trex1*^{-/-} MEFs or WT and *TREX1*^{R114H/R114H} human fibroblasts with three additional RNA viruses that contain either positive- or negative-stranded genomes, and measured levels of viral RNA, amounts of viral proteins, and viral titers in the supernatant. All three viruses, namely influenza virus (A/WSN/1933 strain), Sendai virus (SeV) and West Nile virus (WNV/TX02 strain), failed to replicate efficiently in *Trex1*^{-/-} or *TREX1*^{R114H/R114H} cells compared to WT cells (Fig. 2). These results demonstrate that cells lacking Trex1 function are resistant to infection with several different types of RNA viruses.

Trex1 regulates IFN-independent activation of ISGs

Next, we investigated the mechanism of antiviral resistance in *Trex1*^{-/-} cells. We first examined gene expression profiles by isolating total RNA from WT or *Trex1*^{-/-} MEFs that were mock-infected or infected with VSV, influenza virus, Sendai virus or West Nile virus, and performed RNA-SEQ analysis, which offers quantitative measurement of both host and viral RNAs simultaneously (Fig. 3a). Gene expression fold-change values validated by qPCR were remarkably similar to those from RNA-SEQ (Fig. 3b, Supplementary Fig. 3, data not shown), which underscores the quantitative power of our RNA-SEQ analysis. We first analyzed gene expression profiles of uninfected WT and *Trex1*^{-/-} samples by Ingenuity Pathway Analysis (IPA) and found that the most enriched gene network in *Trex1*^{-/-} cells compared to WT cells is ‘antimicrobial response, inflammatory response, infectious diseases’ consisting mostly of ISGs (Supplementary Fig. 5a,b). ‘Interferon signaling’ and ‘cytosolic pattern recognition receptors’ are also among top ranked canonical pathways with high ‘hit ratio’ (determined by the percentage of genes in a pathway that are represented in a dataset, Supplementary Fig. 5c). We then constructed a heatmap of genes involved in ‘antimicrobial response’ network based on expression values and standard deviations of each gene across all samples (Fig. 3a). All four RNA viruses replicated less efficiently in *Trex1*^{-/-} cells (Fig. 3a lower panel, Supplementary Fig. 4), with values ranging from 4–22% of those observed in WT cells. We also found that many ISGs, such as *Ifit1*, *Ifit3*, *Isg15*, *Zbp1*, and *Usp18*, were highly induced in uninfected *Trex1*^{-/-} cells (Fig. 3b, Supplementary Fig. 3). Remarkably, uninfected *Trex1*^{-/-} cells display an ISG activation signature that resembled infected WT cells (Supplementary Fig. 6), suggesting that the lack of Trex1 function alone is enough to initiate an antiviral state. The establishment of this antiviral state appeared to be independent of IFN, because we did not detect any activation of IFN genes or IFN proteins (Fig. 3c, Supplementary Fig. 3). Moreover, *Ifnb* mRNA induction patterns by different viruses were indistinguishable between WT and *Trex1*^{-/-} cells (Fig. 3d; influenza virus is known to inhibit IFN activation²³). In contrast, *Ifit1* mRNA was low in WT cells and increased after viral infection, whereas *Trex1*^{-/-} cells started with very high *Ifit1* (that appeared to be at a level that is equivalent to that observed in infected WT cells), and it remained high after viral infection (Fig. 3e). *Trex1*^{-/-} cells treated with increasing dose of recombinant IFN-β showed further increase of *Ifit1* expression, suggesting that *Trex1*^{-/-} cells are capable of responding to IFN signaling (Supplementary Fig. 7). ISGs that were highly induced by Trex1 deficiency such as IFIT family members have intrinsic antiviral activity against RNA viruses^{24,25}. Of note, not all known ISGs are activated in *Trex1*^{-/-} cells; IFITM family members were expressed at similar amounts in WT and *Trex1*^{-/-} cells (Supplementary Fig. 3). Together, our data suggested that a subset of ISGs are activated at very high levels in *Trex1*^{-/-} cells independently of the IFN response.

To further confirm that the ISG activation is specific to the loss of Trex1 function, we knocked down Trex1 expression in WT MEFs using three different siRNAs and observed that the expression of *Ifit1*, *Ifit3* and *Irf7* (also an ISG) were increased significantly while the expression of *Ifitm3*, *Ifna4* and *Ifnb1* were not increased (Fig. 3f). We also knocked down Trex1 expression in *Ifnar*^{-/-} MEFs and observed a similar increase in *Ifit1* and *Irf7* expression (Fig. 3g), further suggesting that the ISG activation regulated by Trex1 is IFN-independent. To determine whether the ISG activation or the IFN pathway contributed to

viral infection control in *Trex1*^{-/-} cells, we transfected WT and *Trex1*^{-/-} cells with a control siRNA or a specific siRNA against two ISGs (IFIT1 and IFITM3) or two key components of the IFN signaling pathway (STAT1 and STAT2). We then infected cells with VSV-PeGFP and measured infectivity by FACS (Fig. 3h). The knockdown of IFIT1 and IFITM3 in *Trex1*^{-/-} cells partially alleviated the block in VSV replication, consistent with their known antiviral functions²⁴⁻²⁶. In contrast, STAT1 or STAT2 knockdown had no effect on VSV replication, further demonstrating that the IFN response is not required for control of viral infection in *Trex1*^{-/-} cells. To determine whether this ISG-induction signature occurs in primary immune cells and tissues from *Trex1*^{-/-} mice, we isolated total RNA from whole spleen, heart and BMDMs from WT, *Trex1*^{+/-} and *Trex1*^{-/-} mice and measured *Ifit1*, *Irf7* and *Ifnb* mRNA levels. We observed up to 30-fold induction of ISGs in whole tissues and up to 60-fold induction of ISGs in primary immune cells only in *Trex1*^{-/-} mice compared to WT mice (Fig. 3i). We also observed very low levels of *Ifnb* expression in all samples from *Trex1*^{-/-} mice (Fig. 3i), consistent with a previous report where IFN expression was restricted to a subset of heart muscle cells¹².

We also performed RNA-SEQ to analyze total RNA from uninfected WT or AGS patient fibroblasts carrying mutations in *TREX1* (*R114H/R114H*), or AGS causing genes including *RNASEH2C* (*D39Y/D115fs*) or *SAMHD1* (*R290H/Q548X*)²⁷. We again found strong up-regulation of a subset of ISGs, but not IFN genes, in *TREX1*^{R114H/R114H} cells (Fig. 4a). Interestingly, the ISG activation signature was weak in *RNASEH2C* mutant cells and not present in *SAMHD1* mutant cells (Fig. 4a). To determine whether the same group of ISGs are activated in *Trex1*^{-/-} and *TREX1*^{R114H/R114H} cells, we selected 35 ISGs that are expressed in both mouse and human cells, and compared their induction in *Trex1*^{-/-} versus *TREX1*^{R114H/R114H} cells. ISGs that were induced in *Trex1*^{-/-} MEFs were also induced in *TREX1*^{R114H/R114H} fibroblasts, with a correlation *r*-squared value of 0.49 (Fig. 4b). We observed a weak correlation between gene induction in *Trex1*^{-/-} versus *RNASEH2C*^{D39Y/D115fs} cells (*r*²=0.14) and no correlation in *Trex1*^{-/-} versus *SAMHD1*^{R290H/Q548X} cells (*r*²=0.04). Our data demonstrated that *Trex1* also regulates ISG activation in human fibroblasts.

IFN-independent ISG activation requires STING, TBK1, IRF3 and IRF7

We next wanted to identify innate immune factors that are required for IFN-independent ISG activation in *Trex1*⁻ deficient cells. We chose to measure *Ifit1* mRNA as an example of *Trex1*-regulated ISGs because it is the most highly up-regulated mRNA by *Trex1* deficiency. We first examined IRF3, which activates ISG directly^{9,28}. We measured *Ifit1* mRNA in WT, *Trex1*^{-/-} and *Trex1*^{-/-}*Irf3*^{-/-} MEFs, and found that *Ifit1* is induced in *Trex1*^{-/-} single knockout cells and the induction was inhibited by *Trex1*^{-/-}*Irf3*^{-/-} double knockout, suggesting that IRF3 is required for *Ifit1* activation (Fig. 5a). To determine whether IRF3 is also required for antiviral activity in the setting of *Trex1* deficiency, we infected WT, *Trex1*^{-/-} and *Trex1*^{-/-}*Irf3*^{-/-} MEFs with VSV or SeV, and measured viral proteins by western blot or FACS analysis (Fig. 5b, c, d). Both VSV and SeV infections were inhibited in *Trex1*^{-/-} cells, and both were restored to close to wild-type levels in *Trex1*^{-/-}*Irf3*^{-/-} cells. Therefore, IRF3 is a key component of antiviral resistance in *Trex1*^{-/-} cells. We next wanted to explore which innate immune pathway upstream of IRF3

is involved. IRF3 is activated mostly by cytosolic DNA or RNA sensing pathways that are mediated by STING-TBK1 or RIG-I-MAVS, respectively. Therefore, we knocked down key components of each pathway by siRNAs in *Trex1*^{-/-} cells, and measured *Ifit1* expression. The knockdown of IRF3, IRF7, TBK1, STING, IFI204 significantly reduced *Ifit1* expression, whereas RIG-I and MAVS knockdown had no effect (Fig. 5e). We also did not observe any effect on *Ifit1* expression in *Trex1*^{-/-} cells by knocking down TLR7 or TLR9 (data not shown). IRF3, IRF7 and TBK1 knockdown also decreased the VSV replication block in *Trex1*^{-/-} cells (Fig. 5f). These results suggest that the cytosolic DNA, but not RNA, sensing machinery, is required for IFN-independent ISG activation in *Trex1*-deficient cells. STING knockdown did not appear to increase VSV replication in *Trex1*^{-/-} cells, likely because the VSV replication assay measures the entire life cycle of VSV and many host factors may contribute to it, or because STING also regulates many other genes⁸ that could be required for VSV replication. The same cytosolic DNA sensing pathway is also involved in the activation of IFN genes during viral infection^{2,11}, which can then activate ISGs. Therefore, we performed double knockdowns of *Trex1* plus components of the cytosolic DNA sensing pathway in *Ifnar*^{-/-} MEFs. *Ifit1* expression was increased by *Trex1* knockdown, and this increase was reduced by further knockdown of TBK1, IRF7 OR STING (Fig. 5g). *Trex1* knockdown in *Ifnar*^{-/-} MEFs also inhibited VSV replication, and further knockdown of TBK1 or IRF7 alleviated that inhibition (Fig. 5h). Taken together, our data suggest that the core cytosolic DNA sensing machinery, STING-TBK1-IRF3-IRF7, is involved in activating ISGs directly in cells with reduced or no *Trex1* activity.

Trex1 regulates lysosomal biogenesis through TFEB and mTORC1

We next wanted to identify the underlying basis for ISG activation in *Trex1*^{-/-} or *TREX1*^{R114H/R114H} cells. We first considered the possibility that *Trex1* directly inhibits the cytosolic DNA sensing machinery. To test this, we used 293T cells, in which the overexpression of STING induced a 6-fold increase in levels of *Ifit1* mRNA (Supplementary Fig. 8). We then co-expressed STING and increasing amounts of *Trex1* to examine whether *Trex1* overexpression inhibits STING-mediated *IFIT1* activation. We did not observe any effect on *Ifit1* induction by overexpressing *Trex1* (Supplementary Fig. 8). The same level of *Trex1* overexpression inhibited HIV-mediated activation of IFN genes¹¹. These results suggest that *Trex1* does not directly inhibit the cytosolic DNA sensing machinery.

We then hypothesized that perhaps accumulation of self-ligands or any cellular abnormality in *Trex1*^{-/-} or *TREX1*^{R114H/R114H} cells could be detected by the STING-TBK1-IRF3-IRF7 pathway. We first looked at the abundance and morphology of cellular organelles, comparing WT and *Trex1*^{-/-} cells, by immunofluorescence staining using well-defined organelle markers (Fig. 6a). We did not observe great differences in mitochondria, Golgi, ER, and early endosomes. However, late endosomes (identified by anti-LAMP1 staining) and lysosomes (identified by LysoTracker staining) appeared to be more abundant in *Trex1*^{-/-} cells compared to WT cells (Fig. 6a). Similar increase in the late endosome/lysosome compartment was also observed in *Trex1*^{-/-} BMDMs, but not WT or *Trex1*^{+/-} BMDMs (Fig. 6b). To examine if this is also observed in human cells, we stained WT and *TREX1*^{R114H/R114H} human fibroblasts, or control and *Trex1* knockdown (by siRNAs) HeLa cells with LysoTracker; in both cases, we observed a marked increase in LysoTracker

staining (Fig. 1c, Supplementary Fig. 9), indicating that the late endosome/lysosome compartment is expanded in cells that lack Trex1 function. We quantified lysosome expansion by LysoTracker FACS using live cells; *Trex1*^{-/-} and *TREX1*^{R114H/R114H} cells contained 3–5 fold more lysosomes compared to WT cells (Fig. 6d). We also detected increased LAMP1 and NPC1 (lysosomal membrane proteins) protein level in *TREX1*^{R114H/R114H} and *Trex1*^{-/-} cells compared to WT cells by western blot (Fig. 6e), suggesting enhanced lysosomal biogenesis in Trex1 deficient cells. To further confirm the increase in the lysosome compartment, we analyzed WT and *Trex1*^{-/-} cells by electron microscopy (EM). *Trex1*^{-/-} cells contained significantly more lysosome vacuolar structures (Fig. 6f,g). These structures are surrounded by single-layer membranes, some of which contain electron dense cellular materials that are commonly found in lysosomes (Fig. 6f inset). Lysosomes are important organelles for the breakdown and turnover of other cellular organelles (e.g. mitochondria), proteins and nucleic acids²⁹. Of note, we did not observe excessive accumulation of undigested cellular materials in these lysosomes, which were often found in cells associated with lysosomal storage diseases³⁰. We also did not detect an increase in autolysosomes in *Trex1*^{-/-} cells compared to WT as measured by EM, GFP-LC3 dot formation and by western blots analyzing p62 and LC3 protein levels (Supplementary Fig. 10, data not shown).

To determine whether the lysosome expansion phenotype in *Trex1*^{-/-} cells was caused by the induction of lysosome genes, we measured *Ctsa*, *Sgsh*, *Lamp1*, *Mcoln1* and *Tpp1* expression which encode enzymes or structural proteins of the lysosome. All five genes were up-regulated 3–5 fold in *Trex1*^{-/-} cells compared to WT cells, whereas other non-lysosomal genes did not (Fig. 7a). Many other genes involved in lysosomal biogenesis were also up-regulated in *Trex1*^{-/-} cells compared to WT cells (Supplementary Fig. 11). Lysosome genes are regulated by the transcription factor EB (TFEB) through the recognition of conserved binding sites in their promoters. TFEB is a master regulator of the Coordinated Lysosomal Expression and Regulation (CLEAR) gene network³¹; and its overexpression increases lysosome gene expression and promotes lysosome expansion³². TFEB resides mostly in the cytoplasm and translocates into the nucleus upon complex post-translational modifications^{33,34}. We did not observe any difference in TFEB mRNA or protein amounts in WT and *Trex1*^{-/-} cells (Fig. 7a, data not shown). To examine the subcellular localization of TFEB, we stained WT and *Trex1*^{-/-} cells with anti-TFEB and found that endogenous TFEB became predominately nuclear in *Trex1*^{-/-} cells (Fig. 7b). This result strongly suggests that the increase in lysosomal gene expression and lysosomal compartment expansion were connected to altered TFEB localization in *Trex1*^{-/-} cells. We did not detect any interaction between Trex1 and TFEB by immunoprecipitation from WT MEFs (data not shown), suggesting Trex1 is unlikely to regulate TFEB translocation through direct binding and retention in the cytosol.

To examine whether TFEB function is required for ISG activation and antiviral activity in *Trex1*^{-/-} cells, we knocked down *TFEB* expression in *Trex1*^{-/-} cells and measured *Ifit1* and *Ifit3* mRNA in uninfected cells, and VSV replication in the same knockdown cells. *TFEB* knockdown in *Trex1*^{-/-} cells reduced both *Ifit1* and *Ifit3* expression and increased VSV replication (Fig. 7c, d, e). Knockdown of TFEB in WT MEFs did not affect *Ifit1* or other

innate immune genes that were predicted to be TFEB targets³¹, suggesting that TFEB is unlikely to regulate ISGs directly (Supplementary Fig. 12). Moreover, We found that *Trex1*^{-/-}*Irf3*^{-/-} cells express elevated levels of lysosome genes and LAMP1 protein similar to that in *Trex1*^{-/-} cells, while ISG expression is drastically reduced in *Trex1*^{-/-}*Irf3*^{-/-} cells compared to *Trex1*^{-/-} cells, suggesting that lysosomal biogenesis (regulated by TFEB) acts upstream of ISG expression (regulated by IRF3/7, Supplementary Fig. 11).

TFEB overexpression promotes lysosomal biogenesis³². To examine whether manipulating TFEB expression or nuclear translocation in WT cells also induces ISG expression, we overexpressed TFEB in WT MEFs and found that *Ifit1* expression was increased in a dose dependent manner (Fig. 7f). We also treated WT MEFs with chloroquine, which induces TFEB nuclear translocation³⁵, and observed dose-dependent increase of *Mcoln1* (a lysosomal gene) and *Ifit1* expression (Fig. 7g). These data further support the link between TFEB function in lysosomal biogenesis and ISG induction. Of note, chloroquine treatment of *Trex1*^{-/-} cells did not rescue VSV replication (Supplementary Fig. 13), likely due to its known antiviral effect³⁶⁻³⁸.

One of the upstream regulators of TFEB nuclear translocation is mTORC1, and inhibition of mTORC1 activity under many conditions promotes TFEB nuclear transport^{35,39}. We thus examined mTORC1 activity in infected and uninfected WT and *Trex1*^{-/-} cells. We found that VSV infection induces mTORC1 activity in WT MEFs, consistent with mTORC1 being a pro-viral factor⁴⁰ (Fig. 7h). mTORC1 activity is greatly reduced in both uninfected and infected *Trex1*^{-/-} cells compared to uninfected and infected WT cells (measured by reduced p-S6K, p-S6P and p-4EBP1 levels. Fig. 7h, 7i). We also knocked down mTOR with two independent siRNAs and found that mTOR knockdown in WT MEFs increased *Ifit1* expression (Fig. 7j). Moreover, expression of Flag-Trex1 enhanced mTORC1 activity in WT cells and restored mTORC1 activity in *Trex1*^{-/-} cells compared to vector plasmid controls (Fig. 7k). Our data suggest that Trex1 is important for maintaining mTORC1 activity, and that reduced mTOR leads to ISG induction. Consistent with our data, reduced mTORC1 activity has been associated with antiviral effect⁴⁰. Collectively, our data suggested that Trex1 regulates lysosomal biogenesis through TFEB and mTORC1, and lysosomal biogenesis plays a critical role in innate immunity and antiviral defense (Supplementary Fig. 14).

DISCUSSION

It is well established that IFN plays an important role in antiviral immunity. Our cells are equipped with an extensive network of innate immune sensing mechanisms for detecting invading pathogens through recognition by PRRs. When a PRR is engaged, it triggers a signaling pathway that often leads to the activation of IFN expression³. Infection with enveloped viruses also trigger an IFN-independent pathway that involves the direct activation by IRF3 of a subset of ISGs²⁸. In fact, IRF3 can bind promoters of many ISGs in addition to IFN genes⁴¹. Promoters of IFN genes are complex (e.g. *Ifnb1*), containing both positive and negative regulatory elements for IRFs, NF- κ B and AP-1, and a concerted effort of multiple transcription factors is often required for their stimulation. In contrast, promoters of many ISGs are simpler (e.g. *Ifit1*), and can be easily turned on by IRFs independently of

IFN^{9,41}. Direct activation of antiviral genes is important for nonprofessional IFN-producing cells such as fibroblasts to effectively defend themselves against viral infection, or for cells to defend themselves against viruses that have evolved mechanisms to disrupt the IFN response. It is also advantageous for cells to rapidly induce some ISGs upon viral infection before a stronger and more sustained response can be established by IFN signaling pathways. A recent study of the cytosolic RNA sensing pathway provided strong evidence that IFN-independent activation of ISGs mediated by peroxisomal MAVS is functionally important for defense against RNA virus infections¹⁰.

Very little is known about whether IFN-independent activation of ISGs occurs in the absence of infection, and how it is regulated. Here, we identified Trex1, a cytosolic protein associated with the ER, as a key negative regulator of IFN-independent activation of *Irf1* and other ISGs in uninfected cells. When the function of Trex1 is disrupted, either by genetic knockout in mice, or by a homozygous mutation in humans, or by siRNA knockdown in a variety of cell types, a subset of ISGs were activated independently of IFN, leading to an antiviral state. Remarkably, the ISG induction in Trex1-deficient cells is sustained at very high amounts and achieves an antiviral state that is comparable to that caused by the IFN-dependent pathway. This is in contrast to the viral infection induced IFN-independent response in WT cells that appears to be temporary and less robust¹⁰. We have also challenged WT and *Trex1*^{-/-} mouse cells or *TREX1*^{R114H/R114H} human cells with a variety of RNA viruses including VSV, influenza, Sendai and West Nile virus; and they all failed to replicate in cells that have lost Trex1 function.

We have also identified an innate immune pathway, involving STING-TBK1-IRF3-IRF7 that is important for the IFN-independent ISG activation in Trex1-deficient cells. STING is a critical adaptor protein for sensing pathogen-associated DNA or cyclic di-GMP in the cytosol and subsequent induction of IFN expression^{2,7}. Our data expands the function of the STING-TBK1-IRF3-IRF7 pathway to include both IFN-dependent and independent branches as downstream pathways. A recent study also showed that STING activates STAT6 phosphorylation upon viral infection, which then induces chemokines such as CCL2, CCL20 and CCL26 and immune cell homing⁸. We did not observe induction of these chemokines in *Trex1*^{-/-} or *TREX1*^{R114H/R114H} cells compared to WT (data not shown). Together, STING, and associated innate immune factors are becoming a versatile machinery that can activate multiple distinct downstream pathways.

Our data also shed some light on the potential endogenous trigger of IFN-independent ISG activation. We found that Trex1-deficient or mutant cells contain excessive amount of lysosomal vacuoles and expanded lysosomal compartments as determined by immunofluorescence and immunoblot analysis of lysosomal markers, quantitative RT-PCR analysis of lysosomal genes and by electron microscopy. Consistent with elevated lysosome biogenesis, the master regulator of lysosome genes, TFEB translocates to become predominantly nuclear in *Trex1*^{-/-} cells. We also found that mTORC1 activity is reduced in *Trex1*^{-/-} cells and is restored after Flag-Trex1 expression in *Trex1*^{-/-} cells, suggesting that Trex1 plays an important role in maintaining mTORC1 activity, which regulates TFEB nuclear translocation^{35,39}. We also provided several lines of evidence to demonstrate that TFEB-regulated lysosomal biogenesis is functionally linked to ISG activation: TFEB

knockdown in *Trex1* deficient cells tempered ISG activation and antiviral immunity; TFEB overexpression in WT cells, which promotes lysosomal biogenesis³², increased *Ifit1* expression; chloroquine treatment of WT cells, which induces nuclear translocation of TFEB³⁵ and exhibits antiviral activity^{36–38}, increased *Ifit1* expression up to 15-fold; and mTOR knockdown by siRNA in WT cells also increased *Ifit1* expression. Furthermore, based on our observation of elevated lysosomal genes and protein expression and lack of excess accumulation of undigested contents, *Trex1*^{-/-} cells are likely to have enhanced lysosomal function. One could imagine that the release of abnormally high amounts of processed peptide or nucleic acids into the cytosol, or into the extracellular space (via exocytosis⁴²), might break cellular homeostasis or immune tolerance or exceed the threshold for cytosolic DNA sensing. The exact identity of these cytosolic DNA remains unclear, and previous studies have indicated DNA replication debris²⁰ and endogenous retroelements¹⁹. Aberrant functions of lysosomes have been indicated in lupus nephritis where lysosomal contents mimic viral particles and activate innate immunity⁴³. It is also possible that increased lysosome vacuoles could cause membrane perturbation that would elicit IFN-dependent or -independent antiviral response^{9,44}. Further studies are required to distinguish these possibilities. Together, our work demonstrate an important link between lysosomal biogenesis and innate immune activation of ISGs, as well as a novel role for TREX1 in regulating lysosomal biogenesis through TFEB and mTORC1.

We have previously shown that *Trex1* inhibits HIV-mediated IFN activation¹¹. Here, we validated this finding, and further uncovered a novel function of *Trex1* in the regulation of IFN-independent innate immune activation through lysosomal biogenesis in uninfected cells, which results in a broad-spectrum antiviral state in which the replication of several different RNA viruses is inhibited. Both functions of *Trex1* share a similar innate immune signaling pathway that involves STING-TBK1-IRF3, which can activate multiple downstream pathways. The upstream stimuli for HIV-mediated IFN activation is HIV DNA from nonproductive reverse transcription¹¹, whereas the upstream stimuli for the IFN-independent pathway likely involves lysosome function.

Our work also provides further insight into pathogenetic mechanisms underlying systemic autoimmunity associated with *TREX1* mutation such as SLE, a prototypic autoimmune disease. Central to SLE pathogenesis is that ineffective waste disposal due to impaired apoptosis or defective clearance of cellular debris leads to excessive release of autoantigens which activate innate immune sensors and trigger immune responses leading to formation of autoantibodies⁴⁵. Our findings unravel a novel mechanism for a cell-intrinsic mechanism of initiation of autoimmunity due to enhanced lysosome function. Moreover, the constitutive type I IFN-independent 'ISG-signature' which is detectable in a variety of cell types and tissues may potentially represent a valuable biomarker that could be applied as clinical outcome measure.

In summary, our study uncovered a signaling cascade that involves the biogenesis of a cellular organelle (e.g. lysosome) and cytosolic innate immune detection. Both segments of the cascade function together to establish an antiviral state in *Trex1*-deficient cells independently of IFN activation or viral infection. We identified many components of this cascade, some of which (e.g. TFEB and mTORC1) have not been directly implicated in

intrinsic antiviral immunity. We have also uncovered novel functions of known innate immune regulators such as Trex1 and STING. Further understanding of the mechanism by which this signaling cascade is regulated will have important implications not only for understanding antiviral defense but also pathogenic mechanisms underlying autoimmune diseases.

METHODS

Cells and viruses

Wild-type, *Trex1*^{-/-} and *Trex1*^{-/-}*Irf3*^{-/-} MEFs and *Trex1*^{+/-} mice were provided by D. Stetson (U. Washington) under an agreement with D. Barnes and T. Lindahl. *Ifnar*^{-/-} MEFs were provided by Z. Chen (UT Southwestern). HeLa and 293T cells have been described¹¹. All cells were maintained in Dulbecco's modified Eagle's medium (DMEM) with 10% (v/v) heat-inactivated fetal calf serum (FCS), 2 mM L-glutamine, 10 mM HEPES and 1 mM sodium pyruvate (complete DMEM) with the addition of 100 U/ml penicillin, 100 mg/ml streptomycin and cultured at 37°C with 5% CO₂. WT and AGS human fibroblasts were derived by surgical removal of a piece of skin tissue from healthy donors or AGS patients with indicated mutations, and subsequently cultured in DMEM with 10% (v/v) FCS. For generation of bone marrow-derived macrophages, femurs and tibias were harvested from 8 to 10 weeks old mice. Bone marrow was flushed from the bones with cold DMEM supplemented with 20% L-929 cell-conditioned medium, 10% (v/v) heat-inactivated FCS, 2 mM L-glutamine, 10 mM HEPES, 1 mM sodium pyruvate, 100 U/ml penicillin, and 100 mg/ml streptomycin. Bone marrow cells were cultured in 10-cm petri dishes (10 ml vol) at 37°C, 5% CO₂ for 7 d. At days 3 and 6, fresh medium was added to the cultured cells. Experiments involving human and mouse materials were approved by the Institutional Review Boards of UT Southwestern Medical Center, Dallas, Texas, USA and the Children's Hospital, Technical University Dresden, Dresden, Germany. WT VSV²¹, VSV-PeGFP²¹, influenza virus⁴⁰, Sendai virus⁴⁶, West Nile virus⁴⁷ were generated as described. Cells were infected with the indicated virus, MOI and time points and washed three times with 1X PBS before subsequent analysis. Experiments carried out in BSL2 and BSL3 conditions were approved by the Environmental Health & Safety Committee at UT Southwestern Medical Center.

Reagents and antibodies

Reagents: TRI Reagent, MG132, 3-MA, NH₄Cl, Chloroquine, Wortmannin, Rapamycin (Sigma), Lipofectamine 2000, Vybrant Dil Cell labeling solution, Lysotracker (Invitrogen), mouse interferon ELISA kit (PBL interferon source), recombinant mouse interferon β (Millipore). Antibodies: mouse anti-Trex1 (mouse; 1:1,000 dilution; 29; 611987; BD Biosciences), anti-HMGB1 (rabbit; 1:2,000 dilution; ab18256; Abcam), anti-LAMP1 (rabbit; 1:500 dilution; ab24170; Abcam), anti-SQSTM1/p62 (mouse; 1:1,000 dilution; ab56416; Abcam), anti-LC3 (rabbit; 1:500 dilution; NB100-2220; Novus Biologicals), anti-NPC1 (rabbit; 1:1,000 dilution; # 3878-1, Epitomics), anti-Tubulin (mouse; 1:2,000 dilution; B-5-1-2; Sigma), α -VSV (rabbit; 1:4,000 dilution; R4006-F, kind gift from M. Whitt, University of Tennessee Health Science Center, Memphis, TN), anti-TFEB (rabbit; 1:2,000 dilution; generated in house), anti-Influenza A (goat; 1:250 dilution; B65141G, Meridian

Life sciences), anti-Sendai (rabbit; 1:2,000 dilution; PD029, MBL), anti-WNV (rabbit; 20ug total; C19367, Lifespan Biosciences), anti-mTOR (7C10) (rabbit; 1:1,000 dilution; #2983; Cell Signaling), anti-S6 ribosomal protein (5G10) (rabbit; 1:1,000 dilution; #2217; Cell Signaling), anti-phospho-S6 ribosomal protein (Ser235/236) (rabbit; 1:1,000 dilution; #2211; Cell Signaling), anti-phospho-p70 S6 kinase (Thr389) (rabbit; 1:1,000 dilution; #9205; Cell Signaling), anti-phospho-4E-BP1 (Thr37/46) (rabbit; 1:1,000 dilution; #2855; Cell Signaling), anti-4E-BP1 (rabbit; 1:1,000 dilution; #9644; Cell Signaling) and secondary antibodies (1:4,000 dilution; GE Healthcare) were used for immunoblot analysis according to standard protocols.

RNA isolation, qRT-PCR analysis and Cytokine detection assay

Total RNA from different mouse tissues was extracted with the RNeasy Mini kit (Qiagen, # 74104) and total RNA from cells was isolated using TRI Reagent (Sigma) according to the manufacturer's instructions. RNA quantity and quality were confirmed using a NanoDrop® ND-1000 Spectrophotometer. cDNAs were synthesized from 1 µg total RNA using SuperScript® III First-Strand Synthesis (Invitrogen). Real-time PCR was performed using the Power SYBR Green PCR master mix in an ABI-7500 fast real-time PCR machine (Applied Biosystems) with specific gene primers (sequences, Supplementary Table 1, Sigma) and values are presented relative to GAPDH mRNA. Mouse IFN-β protein in culture supernatants was measured by ELISA (42400-1; PBL interferon source) according to the manufacturer's recommendations.

RNA-SEQ and data analysis

Total RNA was isolated from cells using Trizol. The quality of RNA was determined to be RIN=8 or higher by Bio-Analyzer. One microgram of total RNA was used for producing RNA-SEQ cDNA library using standard protocols that include cDNA synthesis, fragmentation, adding adaptors, size selection, amplification and QC (Illumina). SE50 pair-ended sequencing was done using HI-SEQ 2000 (Illumina) with > 18,000,000 reads/sample. Basic data analysis was done using CLC-Biosystems Genomic Workbench analysis programs to generate quantitative data for all genes, including RPKM values, unique and total gene reads, annotated transcripts and detected transcripts, median coverage, chromosomal location, and putative exons. Uninfected WT and *Trex1*^{-/-} dataset were analyzed by Ingenuity Pathway Analysis software package (Ingenuity Systems, Inc). Heat maps were produced by first normalizing RPKM values of each gene by average and standard deviation across all treatment conditions, and then hierarchy-clustered heat maps were generated using Spotfire software.

Immunostaining, fluorescence microscopy and FACS

Cells grown on coverslips were fixed in 4% (wt/vol) paraformaldehyde and were permeabilized and stained by standard protocols. Samples mounted in Vectashield mounting medium containing DAPI (4,6-diamidino-2-phenylindole; Vector Laboratories) were imaged with a Zeiss Imager.M2 fluorescence microscope equipped with AxioVision software. The following antibodies were used for immunostaining; Anti-HSP60 (Santacruz, 13966), anti-GM130 (BD, 610822), anti-calreticulin (Abcam, Ab4-100), anti-EEA1

(Abcam, ab), anti-LAMP1 (Abcam, ab24170), anti-TFEB (generated in house) with Alexa Fluor 488 and 546 tagged secondary antibodies (Invitrogen, A21202, A21206, A10036 and A10040). Live cell fluorescence microscopy was done by growing cells in 35 mm glass bottom dish and imaging with a Zeiss LSM510 confocal microscope. For visualizing VSV infection in live cells, VSV was incubated with 2 mM Vybrant DiI Cell labeling solution (Invitrogen) in PBS for 10 min, followed by Quick Spin Sephadex G-50 column (Roche) purification to remove residual dye. Labeled VSV-DiI virions were subsequently added to target cells, incubated for 1 h before imaging. In some experiments, LysoTracker Green was used to visualize lysosomes in cells with red-labeled virus. For FACS analysis of lysosomes or VSV-PeGFP-infected cells, cells were incubated with LysoTracker Red (40 nmol/ml for 1 hour) or VSV-PeGFP for indicated time point. Cells were then washed 2 times with PBS and fixed with 1% paraformaldehyde. Cell acquisition was performed in a FACS Calibur (BD Biosciences). For all samples, 20,000 events were computed and analyzed by FlowJo software.

Transfections and western blot analysis

Cells were grown on 24-well plates and transfected with 50 nM siRNA (sequences, Supplementary Table 2. Sigma) using Lipofectamine 2000 (Invitrogen) according to manufacturer's instruction. Cells were harvested after 48–72 h and used for infection, or processed for qRT-PCR or western blot analysis. Plasmid transfections were done with Lipofectamine 2000 (Invitrogen) or with Lonza Amaxa nuclearfactor according to manufacture's instructions. For western blot analysis, cells were washed with ice-cold PBS and lysed with 100 μ l of 1X SDS-PAGE reduced sample buffer. Lysates were incubated at 95°C for 5 min prior to resolving by 10% SDS-PAGE. Proteins were transferred to nitrocellulose membranes and immunoblotted with the indicated antibodies. Bands were visualized using either the ECL detection reagent (Pierce) or Supersignal West Pico Chemiluminescence western blotting detection system (Thermo Scientific, Rockford, IL) and exposed to X-ray film. Films were scanned and images were assembled in Photoshop.

Electron Microscopy

Wild-type, *Trex1*^{-/-} MEFs were washed with PBS and fixed in 2% glutaraldehyde (in 0.1 M phosphate buffered saline) for a minimum of 4 hours and post-fixed in 1% osmium tetroxide (in 0.1 M phosphate buffered saline) for 1 hour. After rinsing and dehydrating with graded ethanol solutions (50%, 70%, 95%, 100%), the specimens were infiltrated sequentially with propylene oxide, 1:1 mixture of catalyzed Eponate 12:propylene oxide, and 100% catalyzed Eponate 12. The specimens were then embedded in embedding molds and polymerized in a 60 °C oven overnight. Thick sections (1.0–1.5 micron) were cut on Leica Ultramicrotome with a glass knife, mounted on glass slides, and stained with toluidine blue stain. Thin sections (60–90 nm) were cut using a Leica Ultramicrotome with a diamond knife, mounted on copper grids, and stained with uranyl acetate and lead citrate. Ultrastructural examination was performed on a Hitachi H-7500 Transmission Electron Microscope.

Statistical methods

Data are presented as the mean \pm s.d. Statistical significance was determined by Student's *t*-test. P values of less than 0.05 were considered statistically significant.

Supplementary Material

Refer to Web version on PubMed Central for supplementary material.

Acknowledgments

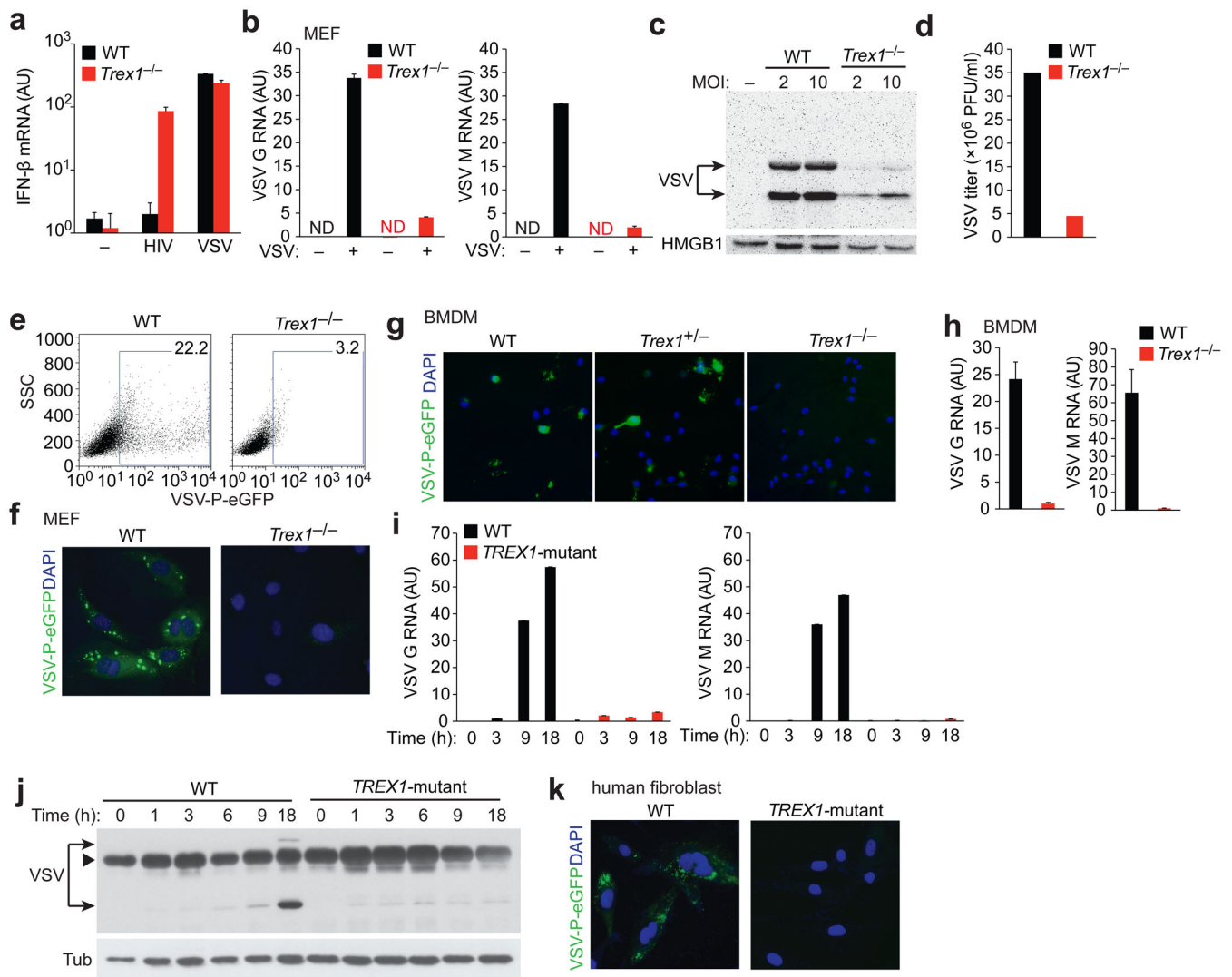
We thank D. Stetson (University of Washington) for wild-type, *Trex1*^{-/-} and *Trex1*^{-/-}*Irf3*^{-/-} primary MEFs and *Trex1*^{+/-} mice, under agreement with D. Barnes and T. Lindahl (Cancer Research UK); We thank R. Orchard and N. Alto (UT Southwestern) for assistance with live cell confocal microscopy; R. Sumpter (UT Southwestern) for assistance with fluorescence microscopy; Z.J. Chen (UT Southwestern) for Sendai virus, *Ifnar*^{-/-} MEFs and valuable discussions; M. Gale (University of Washington) for West Nile virus; B. Fontoura (UT Southwestern) for influenza virus; Z. Zou (UT Southwestern) for technical assistance; M. Whitt for anti-VSV antibody; Electron Microscopy Laboratory at Children's Medical Center for EM studies; J. Lieberman for critical reading of the manuscript and members of the Yan lab for discussions. Supported by the Rita C. and William P. Clements, Jr. Endowed Scholar Award from UT Southwestern to N.Y., the US National Institute of Health (AI093795 and AI098569 to N.Y., CA129387 to J.B., AI057156 to B.L.), The Alliance for lupus research foundation (N.Y.) and Deutsche Forschungsgemeinschaft (LE 1074/4-1 to M. L.-K.).

References

1. Iwasaki A, Medzhitov R. Regulation of adaptive immunity by the innate immune system. *Science*. 2010; 327:291–295. [PubMed: 20075244]
2. Barber GN. Cytoplasmic DNA innate immune pathways. *Immunological reviews*. 2011; 243:99–108. [PubMed: 21884170]
3. Bowie AG, Unterholzner L. Viral evasion and subversion of pattern-recognition receptor signalling. *Nat Rev Immunol*. 2008; 8:911–922. [PubMed: 18989317]
4. Takaoka A, et al. DAI (DLM-1/ZBP1) is a cytosolic DNA sensor and an activator of innate immune response. *Nature*. 2007; 448:501–505. [PubMed: 17618271]
5. Unterholzner L, et al. IFI16 is an innate immune sensor for intracellular DNA. *Nat Immunol*. 2010; 11:997–1004. [PubMed: 20890285]
6. Zhang Z, et al. The helicase DDX41 senses intracellular DNA mediated by the adaptor STING in dendritic cells. *Nat Immunol*. 2011; 12:959–965. [PubMed: 21892174]
7. Burdette DL, et al. STING is a direct innate immune sensor of cyclic di-GMP. *Nature*. 2011
8. Chen H, et al. Activation of STAT6 by STING is critical for antiviral innate immunity. *Cell*. 2011; 147:436–446. [PubMed: 22000020]
9. Noyce RS, Collins SE, Mossman KL. Identification of a novel pathway essential for the immediate-early, interferon-independent antiviral response to enveloped virions. *Journal of virology*. 2006; 80:226–235. [PubMed: 16352547]
10. Dixit E, et al. Peroxisomes are signaling platforms for antiviral innate immunity. *Cell*. 2010; 141:668–681. [PubMed: 20451243]
11. Yan N, Regalado-Magdos AD, Stiggelbout B, Lee-Kirsch MA, Lieberman J. The cytosolic exonuclease TREX1 inhibits the innate immune response to human immunodeficiency virus type 1. *Nat Immunol*. 2010; 11:1005–1013. [PubMed: 20871604]
12. Gall A, et al. Autoimmunity Initiates in Nonhematopoietic Cells and Progresses via Lymphocytes in an Interferon-Dependent Autoimmune Disease. *Immunity*. 2012; 36:120–131. [PubMed: 22284419]
13. Crow Y, et al. Mutations in the gene encoding the 3'-5' DNA exonuclease TREX1 cause Aicardi-Goutieres syndrome at the AGS1 locus. *Nat Genet*. 2006; 38:917–920. [PubMed: 16845398]
14. Crow YJ, Rehwinkel J. Aicardi-Goutieres syndrome and related phenotypes: linking nucleic acid metabolism with autoimmunity. *Hum Mol Genet*. 2009; 18:R130–136. [PubMed: 19808788]

15. Lee-Kirsch MA, et al. Mutations in the gene encoding the 3'-5' DNA exonuclease TREX1 are associated with systemic lupus erythematosus. *Nat Genet.* 2007; 39:1065–1067. [PubMed: 17660818]
16. Lee-Kirsch MA, et al. A mutation in TREX1 that impairs susceptibility to granzyme A-mediated cell death underlies familial chilblain lupus. *J Mol Med.* 2007; 85:531–537. [PubMed: 17440703]
17. Richards A, et al. C-terminal truncations in human 3'-5' DNA exonuclease TREX1 cause autosomal dominant retinal vasculopathy with cerebral leukodystrophy. *Nat Genet.* 2007; 39:1068–1070. [PubMed: 17660820]
18. Moser KL, Kelly JA, Lessard CJ, Harley JB. Recent insights into the genetic basis of systemic lupus erythematosus. *Genes and immunity.* 2009; 10:373–379. [PubMed: 19440199]
19. Stetson DB, Ko JS, Heidmann T, Medzhitov R. Trex1 prevents cell-intrinsic initiation of autoimmunity. *Cell.* 2008; 134:587–598. [PubMed: 18724932]
20. Yang Y, Lindahl T, Barnes D. Trex1 Exonuclease Degrades ssDNA to Prevent Chronic Checkpoint Activation and Autoimmune Disease. *Cell.* 2007; 131:873–886. [PubMed: 18045533]
21. Das SC, Nayak D, Zhou Y, Pattnaik AK. Visualization of intracellular transport of vesicular stomatitis virus nucleocapsids in living cells. *J Virol.* 2006; 80:6368–6377. [PubMed: 16775325]
22. Orebaugh CD, Fye JM, Harvey S, Hollis T, Perrino FW. The TREX1 Exonuclease R114H Mutation in Aicardi-Goutieres Syndrome and Lupus Reveals Dimeric Structure Requirements for DNA Degradation Activity. *J Biol Chem.* 2011; 286:40246–54. [PubMed: 21937424]
23. Kreijtz JHCM, Fouchier RAM, Rimmelzwaan GF. Immune responses to influenza virus infection. *Virus research.* 2011; 162:19–30. [PubMed: 21963677]
24. Pichlmair A, et al. IFIT1 is an antiviral protein that recognizes 5'-triphosphate RNA. *Nat Immunol.* 2011; 12:624–630. [PubMed: 21642987]
25. Yan N, Chen ZJ. Intrinsic antiviral immunity. *Nat Immunol.* 2012; 13:214–222. [PubMed: 22344284]
26. Brass AL, et al. The IFITM proteins mediate cellular resistance to influenza A H1N1 virus, West Nile virus, and dengue virus. *Cell.* 2009; 139:1243–1254. [PubMed: 20064371]
27. Ramantani G, et al. Expanding the phenotypic spectrum of lupus erythematosus in aicardi-goutières syndrome. *Arthritis and rheumatism.* 2010; 62:1469–77. [PubMed: 20131292]
28. Paladino P, Cummings DT, Noyce RS, Mossman KL. The IFN-independent response to virus particle entry provides a first line of antiviral defense that is independent of TLRs and retinoic acid-inducible gene I. *J Immunol.* 2006; 177:8008–8016. [PubMed: 17114474]
29. Saftig P, Klumperman J. Lysosome biogenesis and lysosomal membrane proteins: trafficking meets function. *Nat Rev Mol Cell Biol.* 2009; 10:623–635. [PubMed: 19672277]
30. Cox TM, Cachón-González MB. The cellular pathology of lysosomal diseases. *The Journal of pathology.* 2012; 226:241–254. [PubMed: 21990005]
31. Palmieri M, et al. Characterization of the CLEAR network reveals an integrated control of cellular clearance pathways. *Human molecular genetics.* 2011; 20:3852–3866. [PubMed: 21752829]
32. Sardiello M, et al. A gene network regulating lysosomal biogenesis and function. *Science.* 2009; 325:473–477. [PubMed: 19556463]
33. Settembre C, et al. A lysosome-to-nucleus signalling mechanism senses and regulates the lysosome via mTOR and TFEB. *EMBO J.* 2012; 31:1095–1108. [PubMed: 22343943]
34. Peña-Llopis S, et al. Regulation of TFEB and V-ATPases by mTORC1. *EMBO J.* 2011; 30:3242–3258. [PubMed: 21804531]
35. Rocznik-Ferguson A, et al. The Transcription Factor TFEB Links mTORC1 Signaling to Transcriptional Control of Lysosome Homeostasis. *Science signaling.* 2012; 5:ra42. [PubMed: 22692423]
36. Vincent MJ, et al. Chloroquine is a potent inhibitor of SARS coronavirus infection and spread. *Viol J.* 2005; 2:69. [PubMed: 16115318]
37. Ooi EE, Chew JS, Loh JP, Chua RC. In vitro inhibition of human influenza A virus replication by chloroquine. *Viol J.* 2006; 3:39. [PubMed: 16729896]

38. Savarino A, Boelaert JR, Cassone A, Majori G, Cauda R. Effects of chloroquine on viral infections: an old drug against today's diseases? *Lancet Infect Dis.* 2003; 3:722–727. [PubMed: 14592603]
39. Martina JA, Chen Y, Gucek M, Puertollano R. mTORC1 functions as a transcriptional regulator of autophagy by preventing nuclear transport of TFEB. *Autophagy.* 2012; 8:903–914. [PubMed: 22576015]
40. Mata MA, et al. Chemical inhibition of RNA viruses reveals REDD1 as a host defense factor. *Nat Chem Biol.* 2011; 7:712–719. [PubMed: 21909097]
41. Grandvaux N, et al. Transcriptional profiling of interferon regulatory factor 3 target genes: direct involvement in the regulation of interferon-stimulated genes. *J Virol.* 2002; 76:5532–5539. [PubMed: 11991981]
42. Medina DL, et al. Transcriptional activation of lysosomal exocytosis promotes cellular clearance. *Dev Cell.* 2011; 21:421–430. [PubMed: 21889421]
43. Migliorini A, Anders HJ. A novel pathogenetic concept-antiviral immunity in lupus nephritis. *Nat Rev Nephrol.* 2012; 8:183–189. [PubMed: 22249778]
44. Holm CK, et al. Virus-cell fusion as a trigger of innate immunity dependent on the adaptor STING. *Nat Immunol.* 2012; 13:737–743. [PubMed: 22706339]
45. Marshak-Rothstein A. Toll-like receptors in systemic autoimmune disease. *Nat Rev Immunol.* 2006; 6:823–835. [PubMed: 17063184]
46. Chiu YH, Macmillan JB, Chen ZJ. RNA polymerase III detects cytosolic DNA and induces type I interferons through the RIG-I pathway. *Cell.* 2009; 138:576–591. [PubMed: 19631370]
47. Keller BC, et al. Resistance to alpha/beta interferon is a determinant of West Nile virus replication fitness and virulence. *J Virol.* 2006; 80:9424–9434. [PubMed: 16973548]

**Figure 1.**

VSV replication is impaired in *Trex1* deficient cells. **(a)** Quantitative RT-PCR analysis of IFN- β mRNA in wild type (WT, black bars) and *Trex1*^{-/-} MEFs (red bars) infected with VSV-G pseudotyped HIV-GFP¹¹ or with VSV at an MOI of 2 for 24 h. AU, arbitrary units. ND, not detectable **(b–c)** Quantitative RT-PCR analysis of VSV G and M RNA **(b)**, western blot analysis of VSV proteins **(c)** and virus titers in the supernatants **(d)** of WT and *Trex1*^{-/-} MEFs mock-infected or infected with VSV for 18 h. **(e, f)** Fluorescence activated cell sorting (FACS) **(e)** and fluorescent microscopic **(f)** analysis of WT and *Trex1*^{-/-} MEFs infected with VSV-PeGFP²¹ for 18 h. **(g, h)** fluorescent microscopic **(g)** and quantitative RT-PCR analysis of VSV G and M RNA **(h)** in WT, *Trex1*^{+/-} and *Trex1*^{-/-} MEFs infected with VSV-PeGFP **(g)** or VSV **(h)** for 18 h. **(i, j)** Quantitative RT-PCR analysis of VSV G and M RNA **(i)** and western blot analysis of VSV proteins **(j)** in WT and *TREX1*^{R114H/R114H} primary human skin fibroblasts (*TREX1*-mutant, isolated from a healthy donor or from an AGS patient, respectively) at varying times post infection (0–18 hpi). Arrowhead, a non-specific band. **(k)** Fluorescent microscopic analysis of WT and *TREX1*^{R114H/R114H} cells

infected with VSV-PeGFP for 18 h. Data are representative of at least three independent experiments (error bars, s.d.).

Author Manuscript

Author Manuscript

Author Manuscript

Author Manuscript

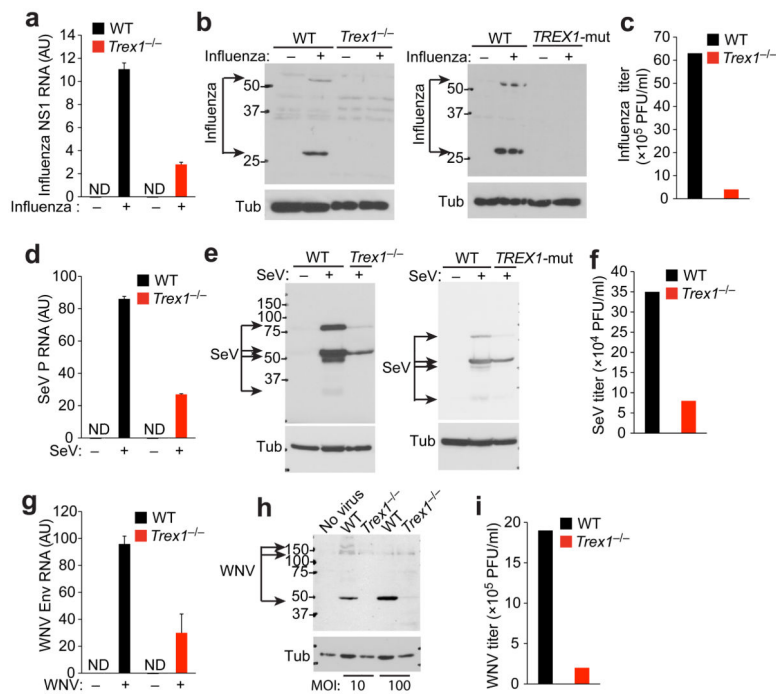


Figure 2. *Trex1* deficient cells display broad antiviral resistance. (a–c) Quantitative RT-PCR analysis of influenza NS1 RNA (a), western blot analysis of influenza proteins (b) and viral titers in the supernatants (c) of WT and *Trex1*^{-/-} MEFs or WT and *TREX1*^{R114H/R114H} (*TREX1*-mut) human fibroblasts infected with influenza virus (A/WSN/1933 strain) at an MOI of 1. AU, arbitrary units. ND, not detectable. (d–f) Quantitative RT-PCR analysis of Sendai virus P RNA (d), western blot analysis of Sendai virus proteins (e) and viral titers in the supernatants (f) of WT and *Trex1*^{-/-} MEFs or WT and *TREX1*^{R114H/R114H} human fibroblasts infected with Sendai virus at MOI of 10. (g–i) Quantitative RT-PCR analysis of West Nile virus Env RNA (g), western blot analysis of West Nile virus proteins (h) and viral titers in the supernatants (i) of WT and *Trex1*^{-/-} MEFs infected with West Nile virus (WNV/TX02 strain) at an MOI of 10 or 100, as indicated. Data are representative of at least two independent experiments (error bars, s.d.).

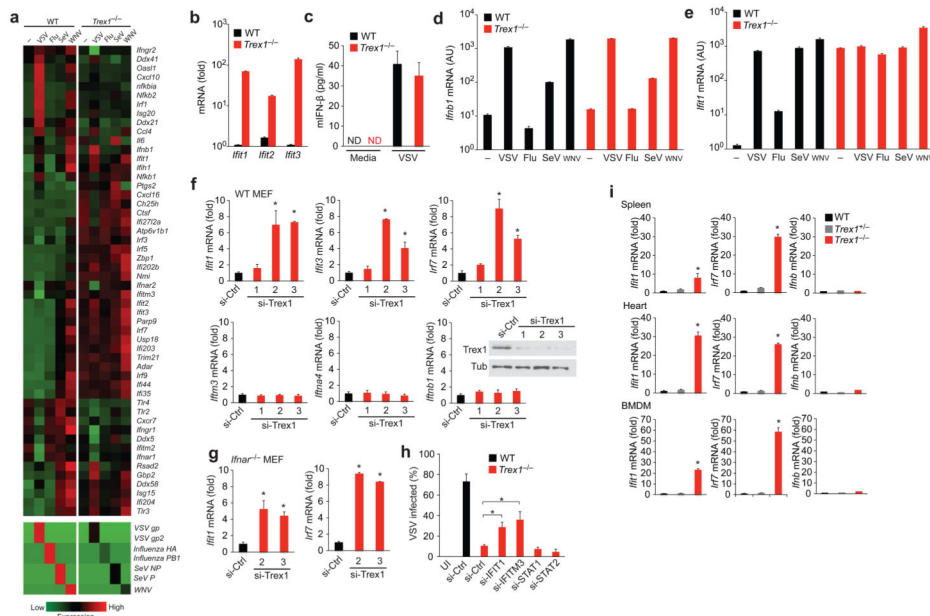


Figure 3. IFN-independent activation of a subset of ISGs in *Trex1* deficient cells. **(a)** A heatmap of selected RNA expression values measured by RNA-SEQ analysis from WT and *Trex1*^{-/-} MEFs uninfected or infected with viruses indicated on top for 18 h. **(b)** Quantitative RT-PCR validation of IFIT family gene expression in uninfected WT and *Trex1*^{-/-} MEFs. **(c)** Mouse IFN- β protein measured by ELISA in supernatants from WT and *Trex1*^{-/-} MEFs uninfected (‘Media’) or infected with VSV. ND, not detectable. **(d, e)** Quantitative RT-PCR validation of *Ifnb1* **(d)** and *Ifit1* **(e)** mRNA levels in WT and *Trex1*^{-/-} MEFs mock-infected or infected with indicated virus. AU, arbitrary units. **(f)** Quantitative RT-PCR analysis of selected ISGs and IFN genes in WT MEFs 72 h after transfection with a control siRNA or *Trex1*-specific siRNAs. si-Ctrl was normalized to 1 in all panels. **P* < 0.05 (Student’s *t*-test). Data are representative of three independent experiments (error bars, s.d.). Insert shows western blot analysis of *Trex1* knockdown. **(g)** Quantitative RT-PCR analysis of *Ifit1* in *Ifnar*^{-/-} MEFs 72 h after transfection with a control siRNA or *Trex1*-specific siRNAs. si-Ctrl was normalized to 1. **P* < 0.05 (Student’s *t*-test). Data are representative of three independent experiments (error bars, s.d.). **(h)** FACS analysis of VSV-PeGFP replication in WT and *Trex1*^{-/-} MEFs transfected with indicated siRNA. Cells were transfected with siRNA for 48 h and mock-infected or infected with VSV-PeGFP for 18 h before FACS analysis. Percentages of GFP positive cells are shown. **P* < 0.05 (Student’s *t*-test). Data are representative of two independent experiments (error bars, s.d.). **(i)** Quantitative RT-PCR analysis of *Ifit1*, *Irf7* and *Ifnb1* mRNA in spleen, heart and BMDM isolated from WT, *Trex1*^{+/-} and *Trex1*^{-/-} mice. **P* < 0.05 (Student’s *t*-test). Data are representative of two independent experiments (error bars, s.d.).

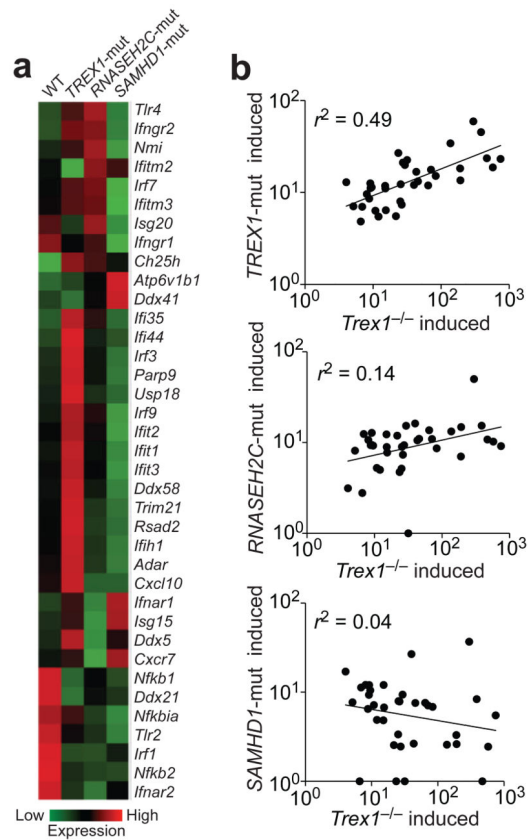


Figure 4.

Selective ISG activation in *TREX1* mutant fibroblasts. **(a)** A heatmap of selected RNA expression values measured by RNA-SEQ analysis from skin fibroblasts isolated from a healthy donor (WT) or from AGS patients carrying mutations in *TREX1* (*R114H/R114H*), *RNASEH2C* (*D39Y/D115fs*) or *SAMHD1* (*R290H/Q548X*). **(b)** Correlation analysis of ISGs induced by *Trex1* deficiency in MEFs versus AGS mutations in humans. Thirty-five ISGs that were expressed in both human and mouse cells were selected for the dot plot. Each dot represents a gene: the x-axis value is fold-increase in *Trex1*^{-/-} MEFs compared to WT, and the y-axis value is fold-increase in AGS mutant cells compared to WT. *r*-squared values represent the quality of correlation observed by fitting a power trend line through all data points.

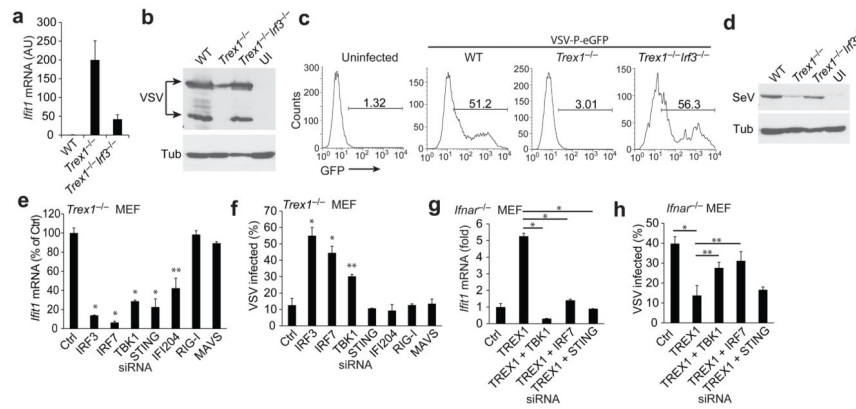


Figure 5. IFN-independent ISG activation in *Trex1* deficient cells requires STING, TBK1, IRF3 and IRF7. **(a)** Quantitative RT-PCR analysis of *Ifit1* in uninfected WT, *Trex1*^{-/-} and *Trex1*^{-/-}*Irf3*^{-/-} MEFs. AU, arbitrary units. **(b)** Western blot analysis of VSV proteins in WT, *Trex1*^{-/-} and *Trex1*^{-/-}*Irf3*^{-/-} MEFs infected with VSV for 18 h. UI, uninfected. **(c)** FACS analysis of VSV replication in WT, *Trex1*^{-/-} and *Trex1*^{-/-}*Irf3*^{-/-} MEFs infected with VSV-PeGFP for 18 h. **(d)** Western blot analysis of Sendai virus proteins in WT, *Trex1*^{-/-} and *Trex1*^{-/-}*Irf3*^{-/-} MEFs infected with Sendai virus for 18 h. **(e,f)** Quantitative RT-PCR analysis of *Ifit1* in uninfected (e), or FACS analysis of VSV-PeGFP infected (f) *Trex1*^{-/-} MEFs transfected with indicated siRNA. *Trex1*^{-/-} MEFs were transfected with indicated siRNAs for 72 h and RNA was extracted for qRT-PCR analysis (e) or infected with VSV-PeGFP for 18 h and analyzed by FACS (f). **P* < 0.01, ***P* < 0.05 (Student’s *t*-test). Data are representative of two independent experiments (error bars, s.d.). **(g,h)** Quantitative RT-PCR analysis of *Ifit1* in uninfected (g), or FACS analysis of VSV-PeGFP infected (h) *Ifnar*^{-/-} MEFs transfected with one or two siRNAs as indicated. **P* < 0.01, ***P* < 0.05 (Student’s *t*-test). Data are representative of two independent experiments (error bars, s.d.).

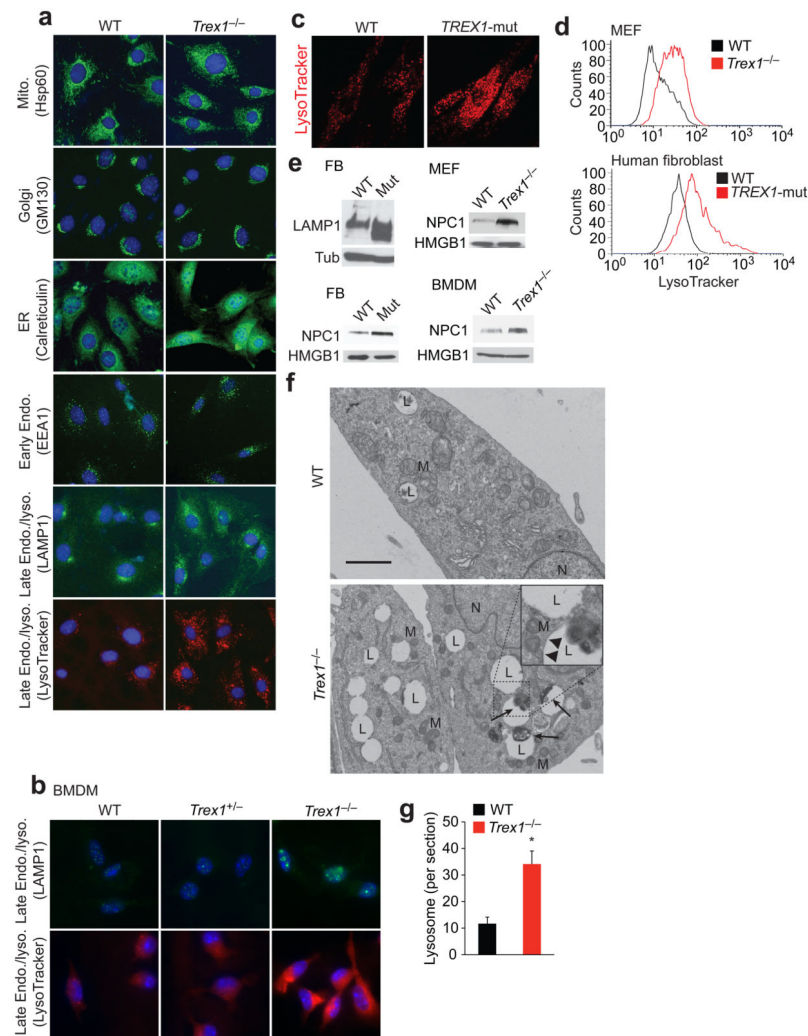


Figure 6. *Trex1* negatively regulates lysosomal biogenesis. **(a-c)** Fluorescent microscopic images of WT and *Trex1*^{-/-} MEFs **(a)** and BMDMs **(b)** stained with indicated organelle markers, WT and *TREX1*^{R114H/R114H} (*TREX1*-mut) human fibroblasts stained with LysoTracker Red **(c)**. **(d)** FACS analysis of live WT and *Trex1*^{-/-} MEFs or WT and *TREX1*^{R114H/R114H} human fibroblasts stained with LysoTracker Red. **(e)** Western blot analysis of lysosomal membrane proteins, LAMP1 and NPC1, in WT and *Trex1*^{-/-} MEFs and BMDMs and WT and *TREX1*^{R114H/R114H} (Mut) human fibroblasts (FB). **(f)** Electron microscopic images of WT and *Trex1*^{-/-} MEFs. The lysosome vacuoles were surrounded by single membrane (arrowheads in insert). Undigested cellular materials (electron dense) were found in some lysosome vacuoles (arrows). N, nucleus. M, mitochondrion. L, lysosome. Scale bar, 1 μ m. **(g)** Number of lysosome vacuoles in thin sections per cell. Averages of 20 cells are shown (error bars, s.d.). * $P < 0.05$ (Student's *t*-test).

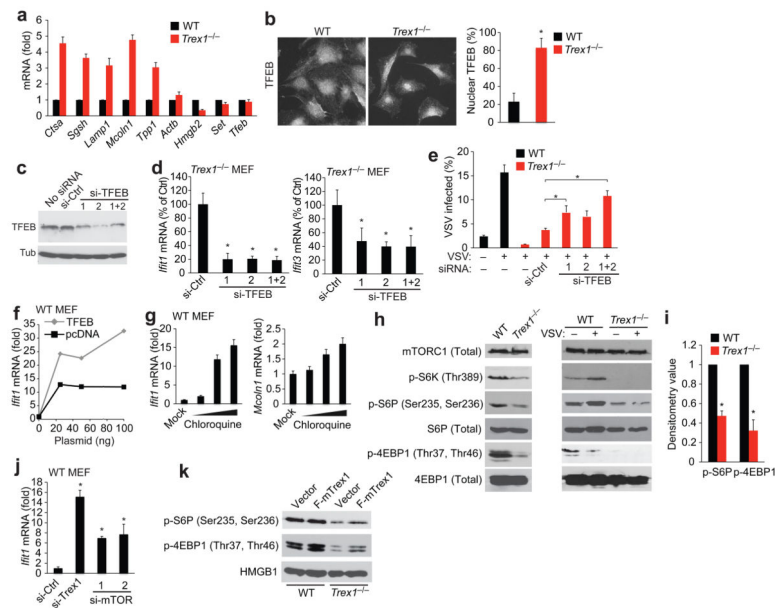


Figure 7.

Trex1 regulates lysosomal biogenesis through TFEB and mTORC1. **(a)** Quantitative RT-PCR analysis of lysosomal and non-lysosomal genes in WT and *Trex1*^{-/-} MEFs. **(b)** Fluorescent microscopic analysis of endogenous TFEB localization in WT and *Trex1*^{-/-} MEFs. Right panel shows percentage of nuclear TFEB in the cell. Averages of 13 cells are shown (error bars, s.d.). **P* < 0.05 (Student's *t*-test). **(c,d)** Western blot analysis of TFEB knockdown **(c)** and qRT-PCR analysis of *Ifit1* and *Ifit3* mRNA **(d)** in *Trex1*^{-/-} MEFs transfected with control or TFEB specific siRNAs. **(e)** FACS analysis of VSV-PeGFP replication in WT and *Trex1*^{-/-} MEFs transfected with control or TFEB specific siRNAs for 72 h and mock-infected or infected with VSV-PeGFP for 18 h. **P* < 0.05 (Student's *t*-test). Data are representative of three independent experiments (error bars, s.d.). **(f)** Quantitative RT-PCR analysis of *Ifit1* expression in WT MEFs transfected with myc-TFEB or pcDNA3 vector plasmid at indicated amount for 24 h. **(g)** Quantitative RT-PCR analysis of *Ifit1* and *Mcoln1* in WT MEFs treated with chloroquine at 10, 50 and 100 uM for 16 h. **(h, i)** Western blot **(h)** and densitometry **(i)** analysis of proteins involved in the mTORC1 pathway. WT and *Trex1*^{-/-} MEFs were uninfected or infected with VSV for 16 h. Densitometry analysis was performed using Image J on 6 independent western blots. WT normalized to 1. **P* < 0.05 (Student's *t*-test). Data are representative of 6 independent experiments (error bars, s.d.). **(j)** Quantitative RT-PCR analysis of *Ifit1* expression in WT MEFs transfected with indicated siRNAs for 72 h. **P* < 0.05 (Student's *t*-test). Data are representative of two independent experiments (error bars, s.d.). **(k)** Western blot analysis of proteins involved in the mTORC1 pathway. WT and *Trex1*^{-/-} MEFs were transfected with vector or Flag-Trex1 plasmid for 24 h. A representative gel image of 4 independent experiments is shown.